Longitudinal L_1 Adaptive Control of a Hypersonic Re-entry Experiment

Zebb Prime[1], Con Doolan[1] and Ben Cazzolato[1]

[1] *School of Mechanical Engineering, The University of Adelaide, Adelaide, South Australia, 5005, Australia*

Abstract

In this paper, the longitudinal flight dynamics of a waverider-class hypersonic vehicle with aerodynamics based on NASA's Generic Hypersonic Aerodynamics Model Example (GHAME) are presented. A brief analysis on the required performance to transition from a re-entry trajectory to horizontal flying is performed, and the results are used as a desired manoeuvre to be achieved in conjunction with a flight controller.

An L_1 adaptive controller is applied to the vehicle to robustly track the desired manoeuvre. The L_1 adaptive controller features fast adaptation, essential for a rapidly changing flight conditions, with a bounded from zero time delay margin for robustness. The ability of the controller to robustly track the manoeuvre is demonstrated through various failure modes and modelling error simulations, such as degradation of control surface effectiveness, reduced longitudinal stability margins and controller processing delays. The simulation results show the L_1 adaptive controller is able to maintain stability during the different scenarios, with some performance degradation for the off-nominal scenarios.

Keywords: L_1 Adaptive Control, Adaptive Control, Robust Control, Hypersonic Control

Introduction

Hypersonc flight control is a challenging research area because it needs to deal with large flight envelopes, reduced stability, rapidly changing and uncertain aerodynamic coefficients, aerothermoelasticity, and many other adverse effects [1,2]. To address these unique requirements, controller methodologies that are robust to uncertainties and able to deal with large parameter variations and nonlinearities are required.

Two current hypersonic experimental programs are the HIFiRE program [3], run by the Defence Science Technology Organisation (DSTO) and partners including the US Air Force Research Laboratory (AFRL), and the SCRAMSPACE program [4], run by the University of Queensland, with partners including the University of Adelaide, whose contribution to the SCRAMSPACE program is to build capability and perform research in hypersonic vehicle flight dynamics, control algorithms and control effectors.

Recently, there has been much research interest in longitudinal control of scramjet powered waverider class hypersonic flight vehicles with an emphasis on the effects of aeroelastic and

attitude on the propulsion system. This work is often based on the model by Ref. 2, and has had a variety of control systems designed to perform all-in-one stability augmentation and trajectory following, including, of particular relevance to this work, an L_1 Adaptive controller [5]. A similar integrated stability and trajectory control LPV controller was applied to a SCRAMSPACE style re-entry vehicle [6], however aeroelastic effects and the scramjet effects were neglected.

Instead of an integrated control structure applied to a free-flying flight experiment, the work presented in this paper will focus on the construction of a fast and robust inner-loop control augmented stability (CAS) controller applied to a waverider style vehicle with aerodynamic control surfaces following a free-flying re-entry trajectory, similar to the HiFIRE 4 payload [3]. The primary control objective of HIFiRE 4 is to perform a pull-up manoeuvre from a flight path angle of approximately $\gamma = -70°$ to $\gamma = -50°$ during the test window of altitudes between $h = 88$ km to $h = 29.5$ km, with a secondary experiment to continue the pull-up manoeuvre until the vehicle is horizontal [7].

This paper is formatted as follows; first the vehicle model and flight dynamics will be introduced, which is then followed by a detailed description of the flight profile and various simulation scenarios that will be used to demonstrate the performance of the controller. An L_1 adaptive controller will then be derived for the flight vehicle and simulation results will be presented before concluding remarks are made.

Re-entry Vehicle Model and Flight Dynamics

The re-entry vehicle used in this analysis is based on the same physical properties of the HIFiRE 4 vehicle, as published in Ref. 7, the values of which are shown in Table 1. The aerodynamic coefficients used in this work are taken from NASA's Generic Hypersonic Aerodynamics Model Example (GHAME), which can be found in Ref. 8. The GHAME aerodynamic database is used as it provides a comprehensive set of lookup tables describing the aerodynamic coefficients of a waverider configuration hypersonic vehicle over the flight conditions with Mach numbers $M \in [0.4\ \ 24]$, and angles of attack $\alpha \in [-3\ 21]°$.

Table 1: Physical properties of the flight vehicle

Mass, m	93.1kg
Inertia, I_{yy}	30 kg.m^2
Planform area, S	0.78 m^2
Characteristic length, c	1.99 m

The flight dynamics of the vehicle are simulated in Mathworks Simulink using the Aerospace Blockset toolbox, using a longitudinally constrained Earth Centric Earth Fixed (ECEF) 6 degree of freedom equations of motion [9] (there are effectively 3 degrees of freedom), based on the World Geodetic System 1984 (WGS-84) Earth and gravity model, with the 1976 Committee on Extension to the Standard Atmosphere (1976 COESA) atmospheric model, 1986 COSPAR International Reference Atmosphere (CIRA-86) zonal wind model, and a Dryden turbulence model based on the MIL-F-8785C specification with a light probability of high-altitude intensity.

Flight Profile and Failure Modes

The flight profile of the re-entry vehicle begins at the same nominal start conditions of the endo-atmospheric control experiment of HIFiRE 4, as shown in Table 2. As the aerodynamics used in this study differ from those of the HIFiRE 4 vehicle, so too will the flight profile differ. A brief performance analysis is performed below, followed by a description of the simulation scenarios used during the simulation to demonstrate the robustness of the L_1 adaptive control methodology.

Table 2: Initial flight conditions of the controller test, based on the starting conditions of the HIFiRE 4 endo-atmospheric test [7]

Mach	7.9
Flight path angle, γ	$-70°$
Altitude, h	88 km

Flight Profile Performance Analysis

A performance analysis was performed on the flight vehicle by simulating the pull-up manoeuvre using the analytic point-mass longitudinal flight dynamics [9,10]:

$$\dot{V} = \frac{1}{m}\left(\frac{(mV\cos\gamma)^2}{Re+h}\sin\gamma - D - mg\sin\gamma\right) \tag{1}$$

$$\dot{\gamma} = \frac{1}{mV}\left(\frac{(mV\cos\gamma)^2}{Re+h}\cos\gamma + L - mg\cos\gamma\right) \tag{2}$$

$$\dot{h} = V\cos\gamma \tag{3}$$

where V is the vehicle velocity; m is the vehicle mass; γ is the flight path angle; Re is the radius of Earth; h is the vehicle altitude; D is the aerodynamic drag; g is the local acceleration due to gravity; and L is the aerodynamic lift. The analysis begins at the flight conditions specified in Table 2, with the angle of attack acting as an input to the system, and the normal z acceleration acting as an output to be limited. The angle of attack was limited to $\alpha_{\max} = 21°$, as this was the maximum in the GHAME database, and the simulations were repeated for several values of the maximum allowable normal acceleration, ranging from 5 to 35 ‘g’ forces in 5 ‘g’ force increments. As the objective of the performance analysis is to determine the ability of the pull-up manoeuvre to take the flight vehicle from a ballistic trajectory to horizontal flight, the flight path angle is plotted as the independent variable in the results shown in Figure 1.

The results in Figure 1 show that to prevent an excessively high dynamic pressure and velocity loss, the vehicle is required to go through a 20–25 ‘g’ force maximum pull-up manoeuvre, with diminishing returns above these values. Although the heating loads and elevon hinge moments have not been calculated in these scenarios, it is expected that these will also demonstrate the requirement for a high normal acceleration manoeuvre.

Based on these results, the controller tests will use a maximum normal acceleration of 25 ‘g’ during the pull-up manoeuvre, and will approximately follow the trajectory shown as the dark blue line in Figure 1.

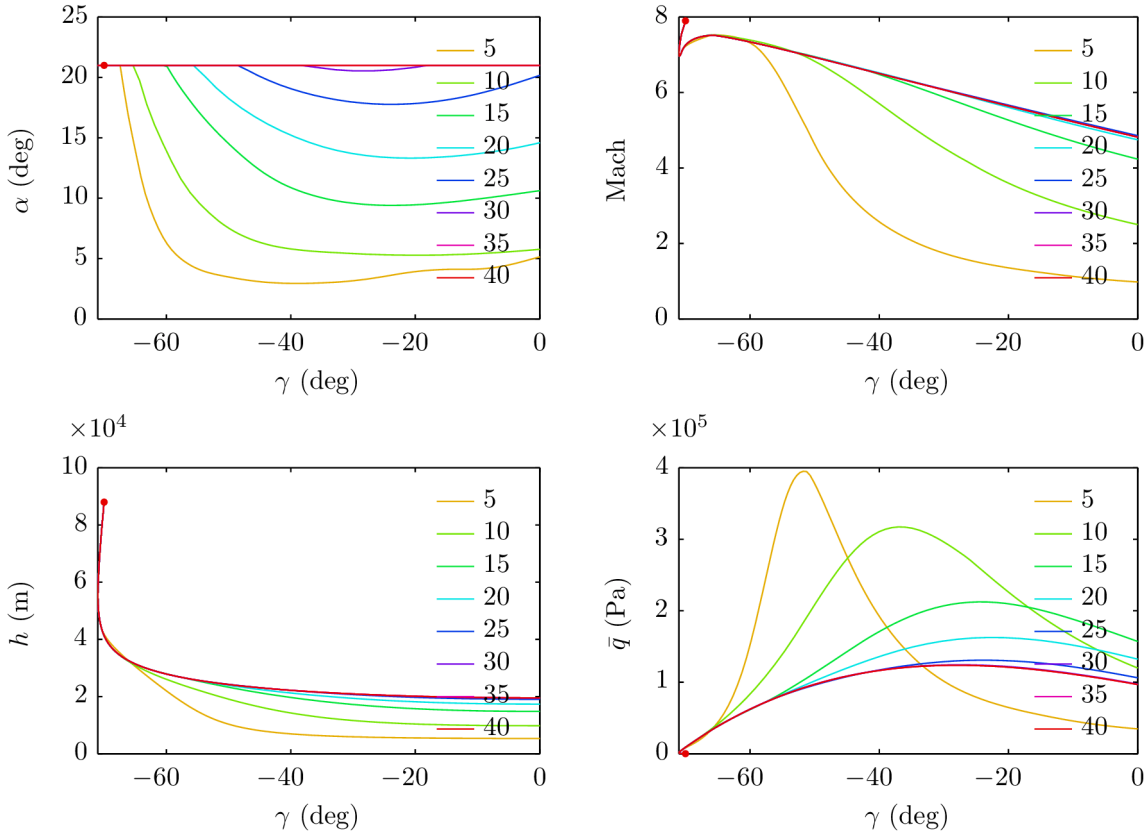

Figure 1: Pull-up performance analysis for different maximum 'g' force loadings, where $\bar{q}$ is the dynamic pressure. Individual lines represent different maximum 'g' force loadings. For values where $\alpha = \alpha_{\max}$, the maximum 'g' force loading has not been reached.

Simulation Scenarios

In order to evaluate the robustness of the L_1 adaptive controller, pull-up simulations were performed using several different scenarios with no controller reconfiguration. These scenarios consist are:

1. Ideal system. The aerodynamic parameters are as per the GHAME database, and there are no control processing delays.
2. Ramp reduction from the nominal elevator effectiveness, M_{δ_e} to $0.5M_{\delta_e}$ starting at $h = 28$ km over 5 seconds.
3. Step reduction from the nominal elevator effectiveness, M_{δ_e} to $0.5M_{\delta_e}$ at $h = 28$ km.
4. Reduced static margin, with $C_{M_\alpha} = C_{M_{\alpha,\text{nom}}} + 0.005C_{L_\alpha}$.
5. Controller processing delay of 10 ms.
6. Controller processing delay of 20 ms.

The reduced elevator effectiveness scenarios correspond to a possible failure or degradation of the control surfaces, possibly due to component failures or ablation, similarly the reduced static margin could be due to aerodynamic uncertainty or aerodynamic degradation. The

controller processing delays represent achievable real-world controller processing delays, and demonstrate the bounded away from zero time delay margin of the L_1 adaptive controller.

L_1 Adaptive Controller Design

Controller Structure

A relatively recent development in adaptive control theory is the L_1 adaptive controller structure, which decouples adaptation speed from robustness. Fast adaptation can then be used to achieve excellent performance without sacrificing robustness [11]. The form of L_1 adaptive controller used in this work includes estimations of the so called unmatched uncertainties, matched uncertainties, and control effecter uncertainty. From Ref. 11, for the system:

$$\dot{x}(t) = A_m x(t) + B_m\left(\omega u(t) + f_1\big(t, x(t), z(t)\big)\right) + B_{um} f_2\big(t, x(t), z(t)\big), \quad x(0) = x_0 \tag{4}$$

$$\dot{x}_z(t) = g\big(t, x_z(t), x(t)\big), \quad x_z(0) = x_{z0} \tag{5}$$

$$z(t) = g_0\big(t, x_z(t)\big) \tag{6}$$

$$y(t) = Cx(t) \tag{7}$$

where $x(t) \in \Re^n$ is the state vector; $A_m \in \Re^{n\times n}$ is the stable state matrix describing the *desired* closed-loop dynamics; $B_m \in \Re^{n\times m}$ is the full-rank nominal input matrix such that (A_m, B_m) is controllable; $\omega \in \Re^{m\times m}$ is the unknown system input gain matrix; $u(t) \in \Re^m$ is the control signal; $f_1: \Re \times \Re^n \times \Re^p \mapsto \Re^m$ and $f_2: \Re \times \Re^n \times \Re^p \mapsto \Re^{(n-m)}$ unknown nonlinear functions representing the matched uncertainties and unmatched uncertainties respectively, $B_{um} \in \Re^{n\times(n-m)}$ is the unmatched input matrix, such that $B_m^{\mathrm{T}} B_{um} = 0$ and $\mathrm{rank}([B_m \;\; B_{um}]) = n$; g_0: $\Re \times \Re^l \mapsto \Re^p$ and g: $\Re \times \Re^n \times \Re^n \mapsto \Re^l$ are unknown nonlinear functions continuous in their arguments; $z(t) \in \Re^p$ and $x_z(t) \in \Re^l$ are the output and state vector of the internal unmodelled dynamics respectively; $C \in \Re^{m\times n}$ is a full rank output matrix such that (A_m, C) is observable; and $y(t) \in \Re^m$ is the regulated system output. Under assumptions of boundedness of $f_i(t, 0)$, semiglobal uniform boundedness of partial derivatives, stability of unmodelled dynamics, partial knowledge of the system input gain and stability of matched transmission zeros (for the mathematical definitions of these assumptions, the reader is referred to Section 3.2 of Ref. 11), the L_1 adaptive controller consists of a state predictor, an adaptation law, and a control law. The state predictor is [11]:

$$\dot{\hat{x}}(t) = A_m \hat{x}(t) + B_m\left(\hat{\omega}(t)u(t) + \hat{\theta}_1(t)\,\hat{x}(t) + \hat{\sigma}_1(t)\right) + B_{um}\left(\hat{\theta}_2(t)\hat{x}(t) + \hat{\sigma}_2(t)\right) - K_{sp}\hat{x}(t), \quad \hat{x}(0) = x_0 \tag{8}$$

$$\hat{y}(t) = C\hat{x}(t) \tag{9}$$

where: $\hat{x}(t) \in \Re^n$ is the estimate of $x(t)$; $\hat{\omega}(t) \in \Re^{m\times m}$, $\hat{\theta}_1(t) \in \Re^{m\times n}$, $\hat{\theta}_2(t) \in \Re^{(n-m)\times n}$, $\hat{\sigma}_1(t) \in \Re^m$, and $\hat{\sigma}_2(t) \in \Re^{(n-m)}$ are the adaptive estimates of the system input gain matrix, the parametric uncertainty and input disturbances respectively; and K_{sp} is the state estimator (estimation) gain. The adaptation laws for the above adaptive estimates are [11]:

$$\dot{\hat{\omega}}(t) = \Gamma\,\mathrm{Proj}\Big(\hat{\omega}(t), -(\tilde{x}(t)PB_m)^{\mathrm{T}} u^{\mathrm{T}}(t)\Big), \quad \hat{\omega}(0) = \hat{\omega}_0 \tag{10}$$

(11) $$\dot{\hat{\theta}}_1(t) = \Gamma \,\mathrm{Proj}\left(\hat{\theta}_1(t), -(\tilde{x}(t)PB_m)^{\mathrm{T}}x^{\mathrm{T}}(t)\right), \quad \hat{\theta}_1(0) = \hat{\theta}_{1_0}$$

(12) $$\dot{\hat{\theta}}_2(t) = \Gamma \,\mathrm{Proj}\left(\hat{\theta}_2(t), -(\tilde{x}(t)PB_{um})^{\mathrm{T}}x^{\mathrm{T}}(t)\right), \quad \hat{\theta}_2(0) = \hat{\theta}_{2_0}$$

(13) $$\dot{\hat{\sigma}}_1(t) = \Gamma \,\mathrm{Proj}(\hat{\sigma}_1(t), -(\tilde{x}(t)PB_m)^{\mathrm{T}}), \quad \hat{\sigma}_1(0) = \hat{\sigma}_{1_0}$$

(14) $$\dot{\hat{\sigma}}_2(t) = \Gamma \,\mathrm{Proj}(\hat{\sigma}_2(t), -(\tilde{x}(t)PB_{um})^{\mathrm{T}}), \quad \hat{\sigma}_2(0) = \hat{\sigma}_{2_0}$$

where: $\tilde{x}(t) \triangleq \hat{x}(t) - x(t)$; $P = P^{\mathrm{T}} \in \Re^{n\times n}$ is the solution to the Lyapunov equation $A_m^{\mathrm{T}}P + PA_m = -Q$ for arbitrary $Q = Q^{\mathrm{T}} > 0$; and $\mathrm{Proj}(\cdot,\cdot)$ denotes the projection operator, used to bound the adaptive estimate and for the proofs of stability [11]. Finally, the control law is [11]:

(15) $$u(s) = -KD(s)\hat{\eta}(s)$$

where $K \in \Re^{m\times m}$ and $D(s)$ is a strictly proper $m \times m$ transfer function chosen so for all ω in its chosen bound, Ω, the transfer function:

(16) $$C(s) \triangleq \omega KD(s)\big(\mathrm{I} + \omega KD(s)\big)^{-1}$$

has unity DC gain and is strictly proper and stable; and $\hat{\eta}(s)$ is the Laplace transform of [11]:

(17) $$\hat{\eta}(t) \triangleq \hat{\omega}(t)u(t) + \hat{\eta}_1(t) + \hat{\eta}_{2,m}(t) - r_g(t)$$

with $\hat{\eta}_1(t) = \hat{\theta}_1(t)\hat{x}(t) + \hat{\sigma}_1(t)$; $\hat{\eta}_{2,m}(s) \triangleq \big((s\mathrm{I} - A_m)B_m\big)^{-1}\big((s\mathrm{I} - A_m)B_{um}\big)\hat{\eta}_2(s)$ where $\hat{\eta}_2(t) = \hat{\theta}_2(t)\hat{x}(t) + \hat{\sigma}_2(t)$; and $r_g(s) \triangleq K_g(s)r(s)$ being the reference signal, $r(t) \in \Re^m$, filtered through the prefilter, $K_g(s)$, chosen to achieve the desired tracking response. The prefilter is often chosen to satisfy unity gain through each channel with no cross-coupling, in which case it can be chosen to be $K_g = -(CA_m^{-1}B_m)^{-1}$.

Reference Model and Control Parameters

An important component of L_1 adaptive controller design is the selection of a suitable reference model. For this vehicle, the L_1 adaptive controller is designed to regulate angle of attack, similar to Ref. 12. The reference model becomes:

(18) $$\begin{bmatrix}\dot{\alpha}\\ \dot{q}\end{bmatrix} = \begin{bmatrix}\frac{Z_\alpha}{V} & \frac{Z_q}{V}+1\\ M_\alpha & M_q\end{bmatrix}\begin{bmatrix}\alpha\\ q\end{bmatrix} + \begin{bmatrix}\frac{Z_{\delta_e}}{V}\\ M_{\delta_e}\end{bmatrix}\delta_e$$

where q is the vehicle pitch rate; δ_e is the actuator position; and Z and M are the standard aircraft force and moment coefficients [9]. Suitable reference values were chosen so the Z force coefficients approximated their actual values over the flight envelope, the M moment coefficients were chosen to place the poles of A_m at suitable values for closed-loop performance, and M_{δ_e} was chosen to be approximately the real values at over parts of the flight. The actual values are:

(19) $$A_m = \begin{bmatrix}0 & 1\\ -5 & -4\end{bmatrix}, \quad B_m = \begin{bmatrix}0\\ -15\end{bmatrix}$$

to ensure the closed-loop poles are located at $s = -2 \pm 1j$, and since the angle of attack is the output to be tracked, $C = [1 \quad 0]$. The unmatched input matrix was chosen to be $B_{um} = [1 \quad 0]^{\mathrm{T}}$ to satisfy the requirements outlined above.

Values for the other controller parameters were chosen to be:

$$D(s) = \frac{1}{s} \tag{20}$$

$$K = 15 \tag{21}$$

$$K_g = -(CA_m^{-1}B_m)^{-1} = -0.333 \tag{22}$$

$$K_{sp} = \mathrm{lqr}\left(A_m, -\mathrm{I}_n, \begin{bmatrix} 500 & 0 \\ 0 & 100 \end{bmatrix}, \begin{bmatrix} 1 & 0 \\ 0 & 1 \end{bmatrix}\right) = \begin{bmatrix} -22.4 & 0.339 \\ 0.339 & -6.73 \end{bmatrix} \tag{23}$$

$$\Gamma = 1000 \tag{24}$$

$$P = \mathrm{lyap}(A_m, \mathrm{I}_n) = \begin{bmatrix} 0.550 & -0.500 \\ -0.500 & 0.750 \end{bmatrix}. \tag{25}$$

The bounds of the adaptive parameters were chosen to be:

$$\omega \in \Omega = [0.25 \quad 1.5] \tag{26}$$

$$|\sigma_m| \leq 1.0 \tag{27}$$

$$|\sigma_{um}| \leq 1.0 \tag{28}$$

$$\|\theta_m\|_2 \leq 20 \tag{29}$$

$$\|\theta_{um}\|_2 \leq 20 \tag{30}$$

Practical Considerations

To more accurately represent the dynamics of the system, the dynamics of the elevator were included as a second order system, with a natural frequency of $\omega_n = 25$ rad/s, damping ratio of $\zeta = 0.8$, deflection limits $|\delta_e| \leq 20°$, and slew rate limits $|\dot{\delta}_e| \leq 90$ °/s. Similarly, to better represent real sensors, uniform white noise was added to the output of the dynamic system. The noise was sampled at $T_s = 0.01$ s with power 10^{-7} and different random number seeds for each of the feedback signals.

In order to prevent wind-up of the integrator $D(s)$, the output of $D(s)$ was restricted to the limits of the elevator, as described above. During the flight, the actuators are often saturated, particularly at lower dynamic pressures; hence the use of an anti-windup mechanism dramatically improves tracking performance.

Rather than directly using the reference trajectory from the Flight Profile Performance Analysis section above, the reference angle of attack to be tracked was generated using a slower outer-loop flight path angle controller with normal acceleration override. Both the flight path angle controller and the normal acceleration override controller are implemented as PID controllers with anti-windup (Section 3.5 of Ref. 13) of the form $u(t) = \mathrm{PID}\big(r(t), y(t)\big)$ where $u(t)$ is the output control signal, $r(t)$ is the reference signal, and $y(t)$ is the output signal. The angle of attack reference is then:

$$\alpha_{\mathrm{ref}}(t) = C_{ol} * \left(\mathrm{PID}_{\gamma}\big(0, \gamma(t)\big) + \mathrm{PID}_{a_z}\left(a_{z,\max}, a_z(t)\right)\right), \tag{31}$$

where the subscripts γ and a_z represent the flight path angle and normal override PID controllers respectively; C_{ol} is a single pole lowpass filter with bandwidth $f_{ol} = 0.5$ Hz; and the PID parameters are given in Table 3. Note that little effort was put into tuning the

parameters of these controllers as the objective of this work is to demonstrate the L_1 adaptive controller.

Table 3: Parameters of the flight path angle and normal acceleration override PID controllers

	PID_γ	PID_{a_z}
Proportional gain, K	1 (rad/rad)	0.005 (rad.s^2/m)
Integrator time, T_I	2 (s)	2 (s)
Derivative time, T_D	0.5 (s)	0 (s)
Tracking time, T_T	2 (s)	2 (s)
Derivative coefficient, N	10 (rad/s)	10 (rad/s)
Saturation, $[u_{\max} \quad u_{\min}]$	$[0.367 \quad -0.524]$ (rad)	$[0 \quad -\infty]$ (rad)

Controller Simulations

Results from the controller simulation for each of the scenarios outlined in Simulation Scenarios section are shown in Figure 2.

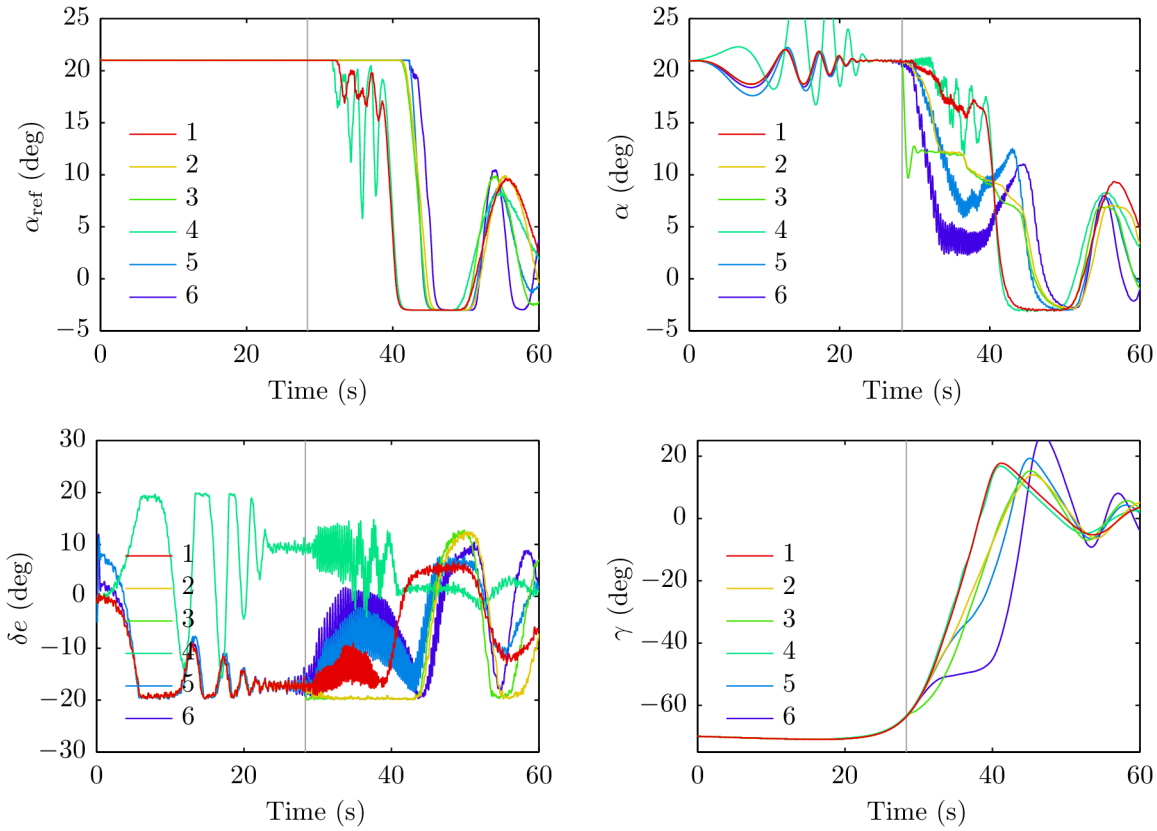

Figure 2: Simulation results of the L_1 adaptive controller. Each of the lines represents one of the simulation scenarios outlined in the Simulation Scenarios section. The grey line represents the start of the controller degradation for scenarios 2 and 3.

The results show that for all scenarios there is some oscillation at the higher altitudes (and low dynamic pressure) due to a mismatch between the controller reference model and the achievable system performance due to the low control authority. As the dynamic pressure increases, the L_1 adaptive controller begins to track the reference angle of attack more accurately. Other simulations show that the controller performance can be improved at low dynamic pressures by reducing the bandwidth and input gains of the reference model, however this comes at the expense of high dynamic pressure performance.

In the effector degradation scenarios (2 and 3), it can be seen that the controller is unable to track the higher angles of attack due to elevator saturation, however once the angle of attack reference is reduced, it again effectively tracks this reference, despite a significant reduction in effector gain. The scenario with reduced longitudinal stability exhibits increased oscillation at low dynamic pressures, but once the dynamic pressure increases, it tracks the angle of attack well due to the increased manoeuvrability associated with the reduced static margin. Note that the oscillations at approximately time $t = 30 - 40$ s are due to the normal override controller. Finally, the scenarios with processing delays exhibit poor performance during the region of high dynamic pressure and high angle of attack requirements, and induce a high-frequency effector requirement; however, once the angle of attack demand is reduced, the controller is able to again effectively track the reference angle of attack.

Notice that the vehicle experiences some flight path angle overshoot towards the end of the simulation. This is due to the outer-loop flight path angle with normal acceleration override controller, and could be improved through further tuning, however this is outside the scope of this work.

Conclusions

In this paper, it has been shown for a hypersonic re-entry vehicle to perform a pull-up manoeuvre to take it from a ballistic to a horizontal trajectory, a high-performance controller is required to maintain high angles of attack to prevent the vehicle experiencing excessive dynamic pressure, which would also correspond to excessive heating load.

An L_1 adaptive controller has been constructed as was shown to be an effective control methodology for the re-entry vehicle, however for some of the off-nominal conditions there was reduced performance, however the vehicle remained stable.

Suggested future work for the control methodology presented in this paper is to use a Linear Time Varying (LTV) [11] reference model to address the trade-off between design for low and high dynamic pressure, as well as a discrete form of the L_1 adaptive controller to guarantee deterministic sampling times [11].

References

1. Bolender, M. and Doman, D., “Modeling unsteady heating effects on the structural dynamics of a hypersonic vehicle”, *AIAA Atmospheric Flight Mechanics Conference*, Keystone, CO, USA, 21–24 August, 2006, AIAA Paper 2006-6646.

2. Bolender, M. and Doman, D., "Nonlinear longitudinal dynamical model of an air-breathing hypersonic vehicle", *AIAA Journal of Spacecraft and Rockets*, Vol. 44, No. 2, 2007, pp. 374–387, DOI: 10.2514/1.23370

3. Dolvin, D., "Hypersonic International Flight Research and Experimentation (HIFiRE): Fundamental sciences and technology development strategy", *AIAA International Space Planes and Hypersonic Systems and Technologies Conference*, Dayton, OH, USA, 28 April–1 May, 2008, AIAA Paper 2008-2581.

4. Tirtey, S., Boyce, R., Brown, L., and Creagh, M., "The SCRAMSPACE I hypersonic flight experiment feasibility study", *AIAA International Space Planes and Hypersonic Systems and Technology Conference*, San Francisco, CA, USA, 11–14 April, 2011, AIAA Paper 2011-2277.

5. Lei, Y., Cao, C., Cliff, E., Hovakimyan, N., Kurdila, A., and Wise, K., "L_1 adaptive controller for air-breathing hypersonic vehicle with flexible body dynamics", American Control Conference, St. Louis, MO, USA, 10–12 June, 2009, DOI: 10.1109/ACC.2009.5160745

6. Prime, Z., Doolan, C., Cazzolato, B., Brooks, L., "Longitudinal flight dynamics modelling and control of ScramSpace I", *AIAA Aerospace Sciences Meeting including the New Horizons Forum and Aerospace Exposition*, Nashville, TN, USA, 9–11 January, 2012, AIAA Paper 2012-0255.

7. Smith, T., Bowcutt, K., Selmon, J., Miranda, L., Northrop, B., Mairs, R., Unger, E., Lau, K., Silvester, T., Alesi, H., Paull, A., Paull, R., and Dolvin, D., "HIFiRE 4: A low-cost aerodynamics, stability, and control hypersonic flight experiment", *AIAA International Space Planes and Hypersonic Systems and Technologies Conference*, San Francisco, CA, USA, 11–14 April, 2011, AIAA Paper 2011-2275.

8. White, D. and Sofge, D., *Handbook of intelligent control*, Van Nostrand Reinhold, New York, NY, USA, 1992.

9. Stevens, B., and Lewis, F., *Aircraft control and simulation*, 2nd Ed., John Wiley and Sons Inc., Hoboken, NJ, USA, 2003.

10. Doolan, C., "Hypersonic missile performance and sensitivity analysis", *AIAA Journal of Spacecraft and Rockets*, Vol. 44, No. 1, 2007, pp. 81–87, DOI: 10.2514/1.23160

11. Hovakimyan, N. and Cao, C., *L_1 Adaptive control theory: guaranteed robustness with fast adaptation*, SIAM, Philadelphia, PA, USA, 2010.

12. Gregory, I., Xargay, E., Cao, C., and Hovakimyan, H., "Flight test of an L_1 adaptive controller on the NASA AirSTAR flight test vehicle", *AIAA Guidance, Navigation and Control Conference*, Toronto, Canada, 2–5 August, 2010, AIAA Paper 2010-8015.

13. Åström, K., and Hägglund, T., *Advanced PID control*, Instrumentation, Systems, and Automation Society, Research Triangle Park, NC, USA, 2006.